Photo-modulation of the two-photon excited fluorescence of dithienylethene bis-(1-pyrenyl) compounds: An experimental and theoretical study

Marie Barale, Iulia Turcas, Violette Gousseau, Muriel Escadeillas, Elsa Caytan, Gregory Taupier, Yann Molard, Arnaud Fihey, Julien Boixel

Dyes and Pigments 232 (2025) 112473

Contents lists available at ScienceDirect

Dyes and Pigments

journal homepage: www.elsevier.com/locate/dyepig

Photo-modulation of the two-photon excited fluorescence of dithienylethene bis-(1-pyrenyl) compounds: An experimental and theoretical study

Marie Barale, Iulia Turcas, Violette Gousseau, Muriel Escadeillas, Elsa Caytan, Gregory Taupier, Yann Molard, Arnaud Fihey **, Julien Boixel *

Université de Rennes, CNRS, ISCR, UMR 6226, ScanMAT, UAR 2025, F-35000, Rennes, France

ARTICLE INFO

Keywords:
Dithienylethene
Pyrene
Photochromism
Two-photon excitation
Computational emission

ABSTRACT

Photomodulation of two-photon excited fluorescence has been effectively controlled in 1-pyrene-based dithienylethenes. The specific molecular design enables photocommutation of two-photon excited fluorescence during sequential one- and two-photon excitations without interference nor destructive optical readout. Theoretical studies have concluded that the internal functionalization of pyrene is responsible for the photoactivity in these systems. Photophysical studies indicate that the presence of a second laterally introduced pyrene is crucial for maintaining high photocommutation contrast and durability.

1. Introduction

Photo-activatable molecules that combine photochromic and fluorescent properties within a single molecule, have garnered increasing interest due to their potential applications in optical memories, molecular switches, and fluorescent biological markers [1–8]. In pursuit of accurately controlling the luminescence signal within a single-molecule, many dithienylethene [9] (DTE)-based systems have relied on intramolecular energy transfer or electron transfer mechanisms [10–17]. These approaches have successfully demonstrated the photoswitching of fluorescence, unfortunately, they encounter the challenge of competition between photo-cyclization and fluorescence emission upon UV light irradiation, along with cycloreversion reactions induced by fluorescence quenching [18–21]. These undesired photochemical processes lead to the destruction of information, deleterious for optical applications. For effective utilization, it is imperative to decouple the photo-switching and luminescence readout processes, enabling independent control over each. In this regard, relying on intramolecular geometrical changes for effective luminescence quenching instead of electron or energy transfer quenching mechanisms appears to be an attractive strategy. Moreover, controlling molecular geometrical changes by light offers the advantage of outstanding spatiotemporal control and has been employed in molecular motors, for example [22,23].

To control a luminescent event through a geometrical change, the formation of an excimeric photo-excited state between two chromophores appears to be an effective strategy. In our exploration of employing dithienylethenes as geometric photo-actuators, we previously explored an innovative DTE compound bearing pyrenes (Chart 1) [24]. With a rational design, this bis-(2-pyrenyl) DTE, can yield photo-switchable excimeric emission. In this system, the photochromic reaction alters the relative orientations of the chromophores, modulating the eximer formation. Furthermore, for the development of all-optical non-destructive readout systems, it is crucial to orthogonally probe the luminescent state to fully utilize the potential of such molecular photo-actuators. This can be achieved by alternating between one-photon excitation (OPE) and two-photon excitation (TPE), selectively triggering the photochromic and luminescent behaviors without interference.

Simultaneous[25–29] and sequential [30–32] two-photon excitation of DTE has been investigated, particularly for enhancing the kinetics of the cycloreversion reaction. This off-resonance TPE typically involves near-infrared light excitation, which reduces photofatigue and has garnered interest for super-resolution microscopy within the biological window. Although this compound demonstrated the ability to switch excimeric emission through photo-induced geometric alterations, its photoluminescence quantum yield was relatively low (PLQY = 5 %),

* Corresponding author.
** Corresponding author.
E-mail address: Julien.boixel@univ-rennes.fr (J. Boixel).

https://doi.org/10.1016/j.dyepig.2024.112473
Received 18 July 2024; Received in revised form 25 September 2024; Accepted 25 September 2024
Available online 27 September 2024

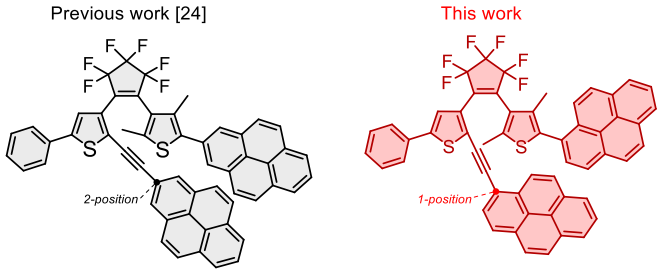

Chart 1. Differences in pyrenyl functionalization between our previous work [24] and this present article.

which diminishes its potential utility. These initial findings have motivated us to delve further into the photo-reactivity of this molecular design, with the aim of optimizing the luminescence output signal. Specifically, we aim to explore functionalization of the pyrenes at their 1-position (Chart 1). It is expected that the enhanced electronic communication through this 1-connection of the pyrene will have a beneficial impact on the photoluminescence behavior. Two mono-pyrenes DTE are also investigated in order to rationalized the effects of the pyrene on their relative lateral or inner positions (Scheme 1, **2TMS** and **3**, respectively).

2. Experimental

2.1. Materials

All reagents for synthesis were obtained from commercial sources and were used as received. Solvents were dried and degassed by standard methods. Tetrahydrofuran was distilled from sodium/benzophenone in a nitrogen atmosphere.

2.2. Synthesis and characterization

2.2.1. Synthesis of 3-bromo-2,4-dimethyl-5-(pyren-1-yl)thiophene (5)

In a dry and argon flushed Schlenk, 2,4-dibromo-3,5-dimethylthiophene (1.81 g, 6.07 mmol) was introduced in dry THF (50 mL) and the solution was cooled to −80 °C. *n*-BuLi 2.5 M (3.25 mL, 6.68 mmol) was added dropwise and the mixture was stirred for 30 min at −80 °C. B$(OBu)_3$ (2.1 mL, 7.8 mmol) was added and the mixture was stirred another 30 min at 0 °C before cannulation in a second Schlenk with an aqueous solution of 1-bromopyrene (2 g, 7.1 mmol), $(Pd(PPh_3)_2Cl_2$ (0.45 g, 0.64 mmol) and Na_2CO_3 (0.63 g, 5.08 mmol) in H_2O (10 mL). The mixture was stirred overnight at reflux. Water (50 mL) was added and the mixture was extracted with dichloromethane and brine. The organic layer was dried over Na_2SO_4 and evaporated. Purification of the crude (SiO_2, dichloromethane/dietylether – 98/2) gave the product as a white solid (2.5 g, 60 % yield). ^{1}H NMR (400 MHz, CD_2Cl_2): δ (ppm) = 8.29–8.20 (m, 3H), 8.19–8.10 (m, 3H), 8.06 (t, J = 7.7 Hz, 1H), 8.00 (dd, J = 8.5, 6.9 Hz, 2H), 2.51 (s, 3H), 1.90 (s, 3H). Elemental analysis: calculated for $C_{22}H_{15}BrS$: C, 67.52; H, 3.86; N, 0.00; S, 8.19. Found: C, 66.90; H, 3.74; N, 0.00; S, 8.28.

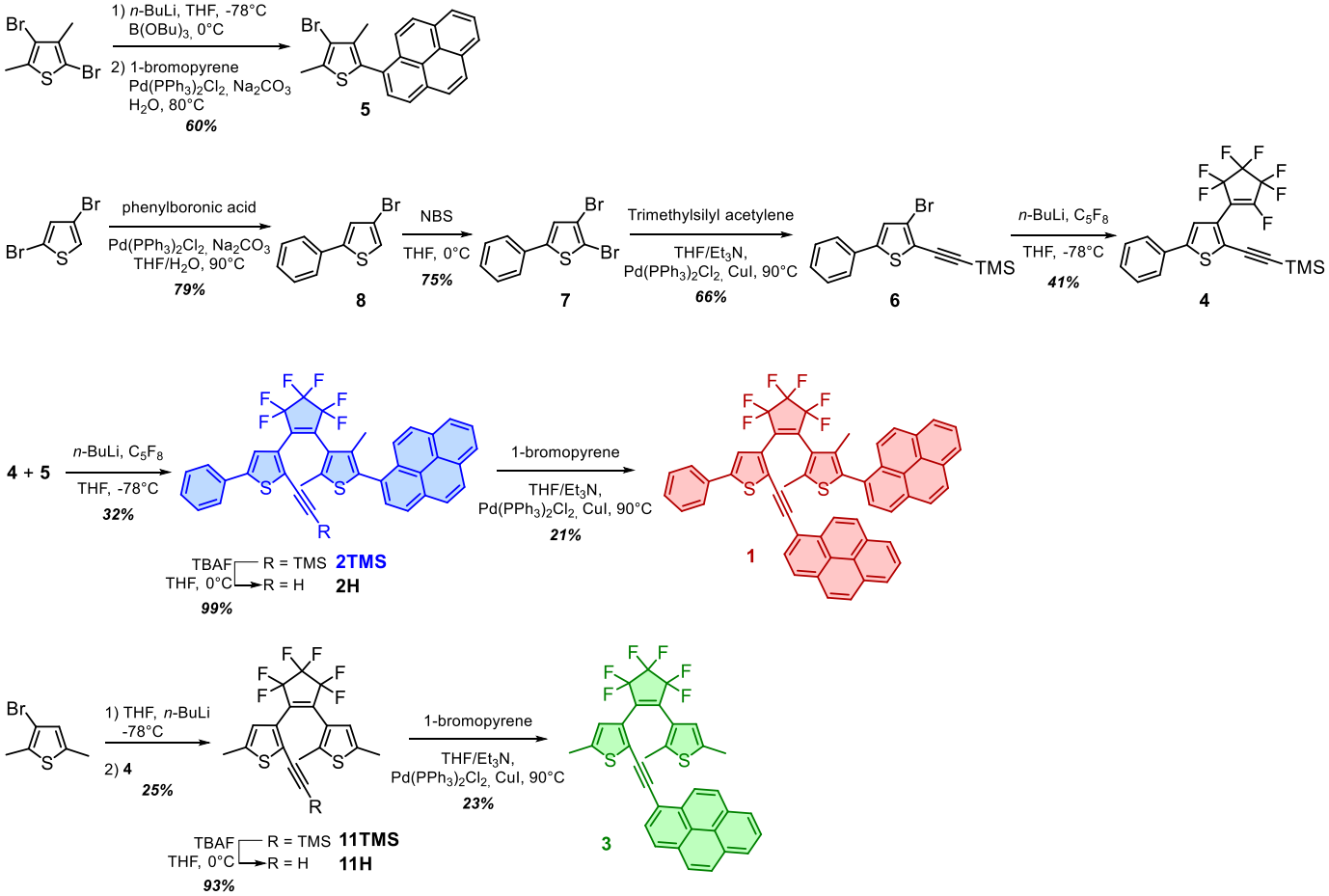

Scheme 1. Synthesis routes for **1**, **2TMS** and **3**.

*2.2.2. Synthesis of 4-bromo-2-phenylthiophene (**8**)*

In a dry and argon flushed Schlenk 2,4-dibromothiophene (3.45 g, 14.26 mmol) and phenylboronic acid (1.74 g, 14.26 mmol) were introduced in dry THF (70 mL) and water (20 mL) and the mixture was degassed with argon bubbling for 30 min. $Pd(PPh_3)_2Cl_2$ (0.60 g, 0.85 mmol) and Na_2CO_3 (1.33 g, 12.55 mmol) were added and the media was heated at 90 °C overnight. Water (50 mL) was added and the mixture was extracted with dichloromethane and brine. The organic layer was dried over Na_2SO_4 and evaporated. Purification of the crude (SiO_2, petroleum ether) gave the product as a white solid (2.70 g, 79 % yield). ^{1}H NMR (300 MHz, $CDCl_3$) δ (ppm) = 7.59–7.53 (m, 2H), 7.43–7.29 (m, 3H), 7.21 (d, J = 1.4 Hz, 1H), 7.17 (d, J = 1.4 Hz, 1H). ^{13}C NMR (101 MHz, $CDCl_3$) δ (ppm) = 145.6, 133.4, 125.9, 125.8, 122.08, 110.7. Elemental analysis: calculated for $C_{10}H_7BrS$: C, 50.23; H, 2.95; N, 0.00; S, 13.41. Found: C, 50.11; H, 3.04; N, 0.00; S, 13.34.

*2.2.3. Synthesis of 2,3-dibromo-5-phenylthiophene (**7**)*

In a dry and argon flushed Schlenk compound **8** (2.06 g, 8.63 mmol) was introduced in dry THF (150 mL) and the solution was cooled at 0 °C. NBS (1.54 g, 8.63 mmol) was added portionwise and the media was stirred overnight. An aqueous saturated solution of $Na_2S_2O_3$ (60 mL) was added and the mixture was extracted with dichloromethane and brine. The organic layer was dried over Na_2SO_4 and evaporated. Purification of the crude (SiO_2, petroleum ether) gave the product as a yellow oil (2.06 g, 75 % yield). ^{1}H NMR (300 MHz, $CDCl_3$) δ (ppm) = 7.53–7.45 (m, 2H), 7.43–7.32 (m, 3H), 7.10 (s, 1H). ^{13}C NMR (101 MHz, $CDCl_3$) δ (ppm) = 122.2, 109.6, 106.0, 105.4, 102.4, 91.4, 86.9. Elemental analysis: calculated for $C_{10}H_6Br_2S$: C, 37.77; H, 1.90; N, 0.00; S, 10.08. Found: C, 37.31; H, 1.76; N, 0.00; S, 11.71.

*2.2.4. Synthesis of ((3-bromo-5-phenylthiophen-2-yl)ethynyl) trimethylsilane (**6**)*

In a dry and argon flushed Schlenk compound **7** (1.99 g, 6.25 mmol) was introduced in dry THF (55 mL) and dry NEt_3 (40 mL). Trimethylsilyl acetylene (1.54 mL, 6.88 mmol) was added and the mixture was degassed with argon bubbling for 30 min. $Pd(PPh_3)_2Cl_2$ (0.22 g, 0.31 mmol) and CuI (0.06 g, 0.31 mmol) were added and the media was heated at 90 °C overnight. An aqueous saturated solution of NH_4Cl (50 mL) was added and the mixture was extracted with dichloromethane and brine. The organic layer was dried over Na_2SO_4 and evaporated. Purification of the crude (SiO_2, petroleum ether) gave the product as a yellow oil (1.73 g, 66 % yield). ^{1}H NMR (400 MHz, $CDCl_3$) δ (ppm) = 7.54–7.51 (m, 2H), 7.41–7.32 (m, 3H), 7.15 (s, 1H), 0.29 (s, 9H). ^{13}C NMR (101 MHz, $CDCl_3$) δ (ppm) = 145.2, 132.8, 129.3, 128.9, 125.9, 125.8), 119.8, 117.4, 104.4, 95.9, −0.03. Elemental analysis: calculated for $C_{15}H_{15}BrSiS$: C, 53.73; H, 4.51; N, 0.00; S, 9.56. Found: C, 53.69; H, 4.49; N, 0.00; S, 9.13.

*2.2.5. Synthesis of trimethyl((3-(perfluorocyclopent-1-en-1-yl)-5-phenylthiophen-2-yl)ethynyl)silane (**4**)*

In a dry argon flushed Schlenk, compound **6** (1.42 g, 4.24 mmol) was introduced in THF (40 mL). The solution was cooled to - 80 °C and *n*-BuLi 2.5 M (1.94 mL, 4.67 mmol) was added dropwise. The solution was stirred for 30 min at - 80 °C. In another dry argon flushed Schlenk, THF (10 mL) was cooled to - 80 °C before introducing C_5F_8 (1.69 mL, 12.73 mmol). The lithiated solution of compound **6** was cannulated dropwise onto a C_5F_8 solution (THF) and the mixture was stirred overnight with the temperature slowly rising to room temperature. Water (50 mL) was added and the mixture was extracted with dichloromethane and brine. The organic layer was dried over Na_2SO_4 and evaporated. Purification of the crude (SiO_2, petroleum ether) afforded the product as a yellow solid (0.79 g, 41 % yield). ^{1}H NMR (400 MHz, CD_2Cl_2): δ (ppm) = 7.64–7.55 (m, 2H), 7.50–7.36 (m, 3H), 7.34 (s, 1H), 0.26 (s, 9H). ^{19}F NMR (396 MHz, CD_2Cl_2): δ (ppm) = −108.21 (dd, J = 12.0, 3.4 Hz, 2F), −118.52 (dt, J = 16.7, 3.3 Hz, 2F), −120.37 to −121.78 (m, 1F), −130.23 (p, J = 4.0 Hz, 2F) ^{13}C NMR (75 MHz, CD_2Cl_2): δ (ppm) = 146.7, 132.9, 129.7, 129.4, 126.5, 122.1, 104.9, 96.8, 18.7, 11.6.

*2.2.6. Synthesis of dithienylethene **2TMS***

In a dry and argon flushed Schlenk, **5** (0.34 g, 0.86 mmol) was introduced in dry THF (30 mL). The solution was cooled to −80 °C, *n*-BuLi 2.5 M (0.38 mL, 0.96 mmol) was added dropwise and the media was stirred for 30 min. A solution of **4** (0.39 g, 0.86 mmol) in dry THF (20 mL) previously cooled to −80 °C was cannulated in the reactive media and the solution was stirred overnight with the temperature slowly rising to room temperature. Water (30 mL) was added and the mixture was extracted with dichloromethane and brine. The organic layer was dried over Na_2SO_4 and evaporated. Purification of the crude (SiO_2, hexane – dichloromethane – 80/20) gave the product as a light-yellow solid (0.21 g, 32 % yield). ^{1}H NMR (400 MHz, CD_2Cl_2): δ (ppm) = 8.20 (dd, J = 8.5, 7.2 Hz, 2H), 8.14–8.05 (m, 3H), 8.05–7.92 (m, 2H), 7.70 (q, J = 11.8, 9.1 Hz, 1H), 7.60–7.54 (m, 2H), 7.50–7.35 (m, 3H), 7.06 (s, 1H), 2.56 (s, 3H), 1.84 (s, 3H), 0.27 (s, 9H). ^{19}F NMR (376 MHz, CD_2Cl_2): δ (ppm) = −104.34 to −114.02 (m, 4F), −130.99 to −136.95 (m, 2F). Elemental analysis: calculated for $C_{42}H_{30}F_6SiS_2$: C, 68.09; H, 4.08; N, 0.00; S, 8.66. Found: C, 67.07; H, 4.14; N, 0.00; S, 8.08. HRMS (*m/z*): $[M+Na]^+$ calcd for $C_{42}H_{30}F_6NaSiS_2$, 763.1360; Found $[M+Na]^+$ 763.1358.

*2.2.7. Synthesis of dithienylethene **2H***

In a dry and argon flushed Schlenk, **2TMS** (0.20 g, 0.27 mmol), was dissolved in 20 mL of THF. The solution was cooled at 0 °C and TBAF (0.30 mL, 0.30 mmol) was added dropwise. After 30 min, the reaction was quenched with water and extracted (dichloromethane). The organic layer was dried over Na_2SO_4 and evaporated. Purification of the crude (SiO_2, hexane) gave the product as a light-yellow solid (0.15 g, 81 % yield). ^{1}H NMR (400 MHz, CD_2Cl_2): δ (ppm) = 8.22 (dd, J = 8.5, 7.2 Hz, 2H), 8.10 (m, 3H), 8.04–7.95 (m, 2H), 7.85 (m, 1H), 7.74 (m, 1H), 7.63–7.61 (m, 2H), 7.45–7.38 (m, 3H), 7.28 (s, 1H), 3.69 (s, 1H), 2.48 (s, 3H), 1.77 (s, 3H). ^{19}F NMR (376 MHz, CD_2Cl_2): δ (ppm) = −107 to −114 (m, 4F), −131 to −137 (m, 2F).

*2.2.8. Synthesis of dithienylethene **1***

In a dry and argon flushed Schlenk, **2H** (0.15 g, 0.23 mmol) and 1-bromopyrene (0.77 g, 0.28 mmol) were introduced in dry THF/NEt_3 (50/30 mL). The mixture was degassed for 20 min before $Pd(PPh_3)_2Cl_2$ (0.008 g, 0.01 mmol) and CuI (0.002 g, 0.01 mmol) were added and the mixture was heated to reflux overnight. Water was added and the mixture was extracted with dichloromethane and brine. The organic layer was dried over Na_2SO_4 and evaporated. Purification of the crude (SiO_2, hexane/dichloromethane – 80/20) gave the product as a yellow solid (0.04 g, 21 % yield). ^{1}H NMR (400 MHz, CD_2Cl_2): δ (ppm) = 8.56 (d, J = 9.1 Hz, 1H), 8.29–7.97 (m, 14H), 7.89 (d, J = 7.8 Hz, 1H), 7.75 (s, 2H), 7.71–7.63 (m, 2H), 7.53–7.39 (m, 3H), 7.27 (s, 1H), 2.41 (s, 3H), 1.78 (s, 3H). ^{19}F NMR (376 MHz, CD_2Cl_2, 300 K): δ (ppm) = −108.08 (d, J = 261.5 Hz, 1F), −109.05 (d, J = 158.1 Hz, 1F), −109.75 (d, J = 166 Hz, 1F), −110.90 (d, J = 261 Hz, 1F), −131.54 (d, J = 240.0 Hz, 1F), −132.56 (d, J = 239.5 Hz, 1F). Elemental analysis: calculated for $C_{55}H_{30}F_6S_2$: C, 76.02; H, 3.48; S, 7.38. Found: C, 73.98; H, 3.71; S, 6.88. HRMS (*m/z*): $[M+Na]^+$ calcd for $C_{55}H_{30}F_6NaS_2$, 891.1585; Found $[M+Na]^+$ 891.1589.

*2.2.9. Synthesis of ((3-(2-(2,5-dimethylthiophen-3-yl)-3,3,4,4,5,5-hexafluorocyclopent-1-en-1-yl)-5-methylthiophen-2-yl)ethynyl) trimethylsilane (**11TMS**)*

In a dry and argon flushed Schlenk, **4** (2.16 g, 5.6 mmol) was introduced in dry THF (70 mL). The solution was cooled to −80 °C, *n*-BuLi 2.5 M (2.6 mL, 5.9 mmol) was added dropwise and the media was stirred for 30 min. A solution of 2-bromo-1,5-dimethylthiophene (1.07 g, 5.6 mmol) in dry THF (30 mL) previously cooled to −80 °C was cannulated in the reactive media and the solution was stirred overnight with the temperature slowly rising to room temperature. Water was

added and the mixture was extracted with dichloromethane and brine. The organic layer was dried over Na_2SO_4 and evaporated. Purification of the crude (SiO_2, hexane) gave the product as a light-yellow solid (0.66 g, 25 % yield). ^{1}H NMR (400 MHz, CD_2Cl_2): δ (ppm) = 6.75 (m, 1H), 6.72 (m, 1H), 2.43 (d, J = 1.2 Hz, 3H), 2.42 (m, 3H), 1.83 (s, 3H), 0.16 (s, 9H). ^{19}F NMR (376 MHz, CD_2Cl_2, 300 K): δ (ppm) = −109.77 (m, 2F), −110.76 (m, 2F), −132.20 (m, 2F).

2.2.10. Synthesis of 3-(2-(2,5-dimethylthiophen-3-yl)-3,3,4,4,5,5-hexafluorocyclopent-1-en-1-yl)-2-ethynyl-5-methylthiophene (11H)

In a dry and argon flushed Schlenk, **11TMS** (0.50 g, 1.04 mmol), was dissolved in 50 mL of THF. The solution was cooled at 0 °C and TBAF (1.04 mL, 1.04 mmol) was added dropwise. After 30 min, the reaction was quenched with water and extracted (dichloromethane). The organic layer was dried over Na_2SO_4 and evaporated. Purification of the crude (SiO_2, hexane) gave the product as a light-yellow solid (0.21 g, 48 % yield). ^{1}H NMR (400 MHz, CD_2Cl_2): δ (ppm) = 6.78 (m, 1H), 6.68 (m, 1H), 3.35 (s, 1H), 2.46 (d, J = 1.4 Hz, 3H), 1.88 (m, 3H). ^{19}F NMR (376 MHz, CD_2Cl_2, 300 K): δ (ppm) = −109.79 (m, 2F), −110.74 (m, 2F), −132.20 (m, 2F).

2.2.11. Synthesis of dithienylethene 3

In a dry and argon flushed Schlenk, **11H** (0.202 g, 0.490 mmol) and 1-bromopyrene (0.152 g, 0.540 mmol) were introduced in dry THF/NEt_3 (120/50 mL). The mixture was degassed for 20 min before Pd$(PPh_3)_2Cl_2$ (0.017 g, 0.025 mmol) and CuI (0.025 g, 0.005 mmol) were added and the mixture was heated to reflux overnight. Water was added and the mixture was extracted with dichloromethane and brine. The organic layer was dried over Na_2SO_4 and evaporated. Purification of the crude (SiO_2, hexane) gave the product as a yellow solid (0.07 g, 23 % yield).

^{1}H NMR (400 MHz, CD_2Cl_2): δ (ppm) = 8.34–7.96 (m, 9H), 6.95 (m, 1H), 6.45 (m, 1H), 2.56 (d, J = 1.2 Hz, 3H), 1.87 (s, 3H), 1.51 (s, 3H). ^{19}F NMR (376 MHz, CD_2Cl_2, 300 K): δ (ppm) = −109.59 (m, 2F), −110.75 (m, 2F), −132.06 (m, 2F). Elemental analysis: calculated for $C_{34}H_{20}F_6S_2$: C, 67.32; H, 3.32; S, 10.57. Found: C, 62.32; H, 4.06; S, 10.88. HRMS (m/z): $[M+Na]^+$ calcd for $C_{34}H_{20}F_6NaS_2$, 629.0803; Found $[M+Na]^+$ 629.0805.

2.3. Measurements

^{1}H, ^{13}C{^{1}H}, ^{19}F{^{1}H} NMR spectra were recorded either on a Bruker Avance III 400 MHz spectrometer equipped with a tunable BBFO probe, or Bruker Avance III HD 500 MHz spectrometers fitted with BBFO or BBO probe (CRMPO or PRISM platforms – Université de Rennes I). Chemical shifts δ are given in ppm and coupling constants J in Hz. ^{1}H and ^{13}C NMR chemical shifts were determined using residual signals of the deuterated solvents, either deuterated dichloromethane (^{1}H δ = 5.32 ppm, ^{13}C δ = 54.0 ppm) or deuterated chloroform (^{1}H δ = 7.26 ppm, ^{13}C δ = 77.16 ppm). The terms s, d, t, q, m indicate respectively singlet, doublet, triplet, quartet, multiplet; b is for broad; dd is doublet of doublets, dt – doublet of triplets, td – triplet of doublets, hept – heptuplet. Assignments of proton carbon signals are based on COSY, NOESY, edited-HSQC, and HMBC experiments. ^{1}H dipolar couplings were studied using NOESY sequence, with 800 ms mixing time. Assignments of fluorine signals are based on ^{19}F COSY, ^{19}F-^{13}C HMQC experiments. ^{1}H-^{19}F through space interactions were studied using 1D-selective or 2D ^{1}H-^{19}F-HOESY experiments, with 500 or 800 ms mixing time, or HXCOSY experiments.

High-resolution mass spectra (HRMS) and Elemental Analysis were performed at the CRMPO (Centre de Mesures Physiques de l'Ouest) in Rennes.

UV/vis absorption spectra were recorded with a Jasco V-770 UV–Vis–NIR spectrophotometer using quartz cuvettes of 1 cm pathlength.

Photoisomerization experiments in solution have been made using a LS series Light Source of ABET technologies, Inc (150 W xenon lamp), with single wavelength light filters "350FS 10–25" or "450FS 40-25" for ring-closure and "650FS 10–25" for cycloreversion. Irradiations for ^{1}H NMR experiments have been made using a Rayonet® with 350 nm light emitting lamps.

Photokinetic time-profiles were recorded using a home-made spectroscopy set-up, which collects absorption spectra at high rates under continuous irradiation of a solution sample, placed in a 1 × 1 cm quartz cuvette under strong stirring, with thermostat control at 20 °C (sample holder LUMA40 from Quantum Northwest). A Hg-Xe lamp from Hamamatsu (Lightningcure LC8, 200 W), equipped with appropriate interferential filters (Semrock) to precisely select the desired wavelength at either 365 nm or 500 nm Hg-lines, was used to photoisomerize the sample. The incident lamp power was measured by means of an Ophir PD300-UV photodiode, subtracting the NIR contribution from the total value. A UV–visible Xenon lamp (75 W) was employed as the probe beam. The transmitted light through the sample was collected by a spectrograph equipped with a CCD camera (Roper Scientific and Princeton Instruments, respectively), the absorption time-profiles at the band maximum of the closed DTE (580 nm) were plotted and fitted using a numerical iterative fitting method, providing the $\Phi_{o\rightarrow c}$ and $\Phi_{c\rightarrow o}$ quantum yields.

All solvent used for photophysical measurements were of spectrometric grade. The absolute quantum yields were measured with a C9920–03 Hamamatsu system. Emission spectra by one- or two-photon absorption were recorded using a femtosecond laser chain (Ti-Sapphire Chameleon ultra II Coherent + pulse picker + SHG module when needed, pulse duration: 100–130 fs; pulse frequency: 5 MHz) and an Ocean optics QEPro CCD detector with integrating times ranging from 6 to 60s. The excitation beam crossed a lens before arriving on the sample and a short-pass filter (FESH0700 from thorlabs) after the sample to remove the excitation signal and prevent damages on the CCD detector. Such filter acts as a band pass filter with a transmission higher than 96 % between 395 nm and 695 nm. The power of the beam was measured with a PMD100 console and a S142C integrating sphere sensor from Thorlabs. For emission intensity vs excitation power measurements, a $\lambda/2$ waveplate and a polarizer were used to vary the laser power. The 2 PE was recorded in solution, perpendicularly to the beam using an optical fiber connected to a CCD detector (QE Pro Ocean Optics). To validate the experimental set-up, the quadraticity (I vs P^2) was first verified on a Coumarin-540a solution at 8.49 10^{-5} M in toluene. Two-photon absorption cross-section values were evaluated using Coumarin-540a as standard with an absolute quantum yield value calculated with the same set-up as the one used for **1** ([Coumarin-540a] = 8.49 10^{-5} M in toluene; [**1**] = 1.6 10^{-6} M in DCM; using σ_2 reference values from Rebane et al. [33].

2.4. Computational methods

All (TD-)DFT calculations have been conducted with the Gaussian 16 software [34], using the global hybrid PBE0 functional [35] and a 6-311+G(d,p) basis set. Ground-state geometry optimizations were followed by frequency calculations to verify the nature of the minimum. Emission energies were obtained by relaxing the geometry of the first excited state, also followed by frequencies calculations. Solvent effects (dichloromethane) were included in all steps through a Polarizable Continuum Model (PCM) [36]. For a discussion of the impact of empirical dispersion model in these calculations, see the dedicated section in the ESI.

3. Results and discussion

3.1. Synthesis and structure

The asymmetrical bis-pyrene DTE **1** is obtained through a converging synthesis (Scheme 1). The strategy is to synthesize the two thiophenic

parts (compounds **4** and **5**) of the DTE separately, allowing their early functionalization at will. The two parts are then combined by sequential nucleophilic substitution to obtain the corresponding mono-pyrene substituted DTE **2TMS**. The deprotection of the acetylenic arm will result in the obtention of the acetylene terminated DTE **2H**, thus allowing a final Sonogashira cross-coupling with the 1-bromopyrene to obtain the targeted bis-pyrene DTE **1(o)**.[23] Following similar synthesis route, the reference compound **3** was prepared.

Complete NMR studies were performed on the DTE-based pyrene compounds **1–3**. Particularly, sets of 2D NMR experiments were conducted on **1**, in order to assign characteristic protons and fluorine atoms (see ESI). Proton signals assigned to protons H2, H3 and H10 are broadened (Fig. 1). One can notice that these broadened signals are also present for compounds **2TMS** and **2H**, but are absent in **3** (see ESI). Such broadening is due to the steric hindrance arising from a rotational constraint with the methyl Me11. This phenomenon is also visible in the ^{19}F NMR spectra which are anomalously broadened. This observation is in line with the computed energy profile along the pyrene/thiophene torsion on the lateral arm (Fig. S10), which shows that the pyrene at the lateral position undergoes clear rotational constrains for torsion angles outside of the 40–140° range, though the energy profile is very flat in this region. For **1(o)**, the computed ground-state geometry exhibits a tilted orientation of the two pyrene moieties by ca. 65° (Fig. S8). This is in clear contrast to the conformation computed on our previous system [24], where the two pyrene units had more space to rearrange and achieve stabilization when oriented towards each other. In **1(o)**, this tilted orientation of the two pyrene units arises from the twisting of the pyrene of the lateral arm compared to the thiophene group by 70°, whereas in the interior arm the more efficient π-conjugation through the acetylene and the absence of steric hindrance induces a pyrene orientation only twisted by ca 20° compared to the thiophene unit. This leads to delocalization of the frontier molecular orbitals of **1(o)** either on the interior arm of the DTE and the attached pyrene (see HOMO and LUMO in Fig. 2) or more on the pyrene of the lateral arm (see HOMO-1 and LUMO+1).

To overcome this rotational barrier, a variable temperature (VT) NMR experiment was performed, recording ^{1}H and ^{19}F NMR spectra of **1(o)** from 300 to 363 K (Fig. 1). The signal of hydrogens H2 and H3 at $\delta =$ 7.77 ppm and H10 at $\delta = 7.92$ ppm gained resolution upon increasing the temperature, meaning the rotational barrier was overcome. However, as no coalescence is observed neither in the proton nor the fluorine NMR spectra, the rotational barrier cannot be experimentally estimated. At high temperature, the better resolution allows the characteristic coupling pattern between the non-equivalent fluorine atoms to be observed. The non-equivalence of ^{19}F nuclei is due to the hindered rotation of methyl bearing thiophene group.

One of the prerequisites for designing these molecular switches is that the two pyrenes must be positioned facing each other, in an anti-parallel conformation of the DTE. Unfortunately, the crystallographic analysis of yellow single crystals, obtained by slow evaporation of a concentrated dichloromethane solution of **1**, shows that in the crystal packing the parallel conformation of the DTE is the most stable, as it is forced by an intermolecular packing between pyrenes (Fig. S7 and Table S1).

To analyze the conformation of **1(o)** in solution, both ^{1}H-^{1}H and ^{19}F-^{1}H through-space correlations have been studied through 2D-NMR experiments (NOESY and HXCOSY) (Fig. S1). ^{1}H-^{1}H NOESY spectrum at room temperature allows the clear assignment of Me11, showing dipolar coupling to the pyrene linked to the same thiophene. Both Me11 and Me12 show dipolar coupling to H1, since thiophene group on the left is rapidly rotating. At low temperature, this rotation is much slower and two distinct conformations can be seen on ^{19}F and ^{1}H spectra (Fig. S2). Scalar couplings arising from spatial proximities between H and F atoms can be investigated using the HXCOSY sequence. For **1(o)** at low temperature, distinctive through-space correlation spots between Me_{11}/F_1 and Me_{12}/F_2 confirm the inhibition of rotation in the "*right*" arm around the thiophene-bridge bond during the NMR timescale.

3.2. Photophysical properties

The electronic absorption spectra of compounds **1**, **2TMS**, and **3**, recorded in dichloromethane, are given in Fig. 3, and pertinent data are summarized in Table 1. A noteworthy observation is that both the number and position (inner or lateral) of the pyrene units significantly influence the ground state absorption spectroscopy. Compound **2TMS**, displays two prominent bands at 360 and 280 nm, lacking vibrational spacing structuration typically observed for 1-substituted pyrenes [37]. The absence of structuration in electronic transitions is ascribed to conformational strain induced by the adjacent methyl group. The other mono-pyrene compound **3**, exhibits an absorption band at 290 nm, akin to the one observed for **2TMS** (at 280 nm). However, it shows a markedly different absorbance in the first transitions, featuring a large and weakly structured band tailing up to 470 nm. This contrast in lower-lying transition, compared to **2TMS**, is attributed to the electronic delocalization along the "arm" from the pyrene to the thiophene [38, 39]. Compound **1(o)** exhibits an absorption spectrum that is essentially a superimposition of the spectra of **2TMS** and **3**, with a notable shift in the lower-lying absorbance band, which appears 25 nm lower in energy.

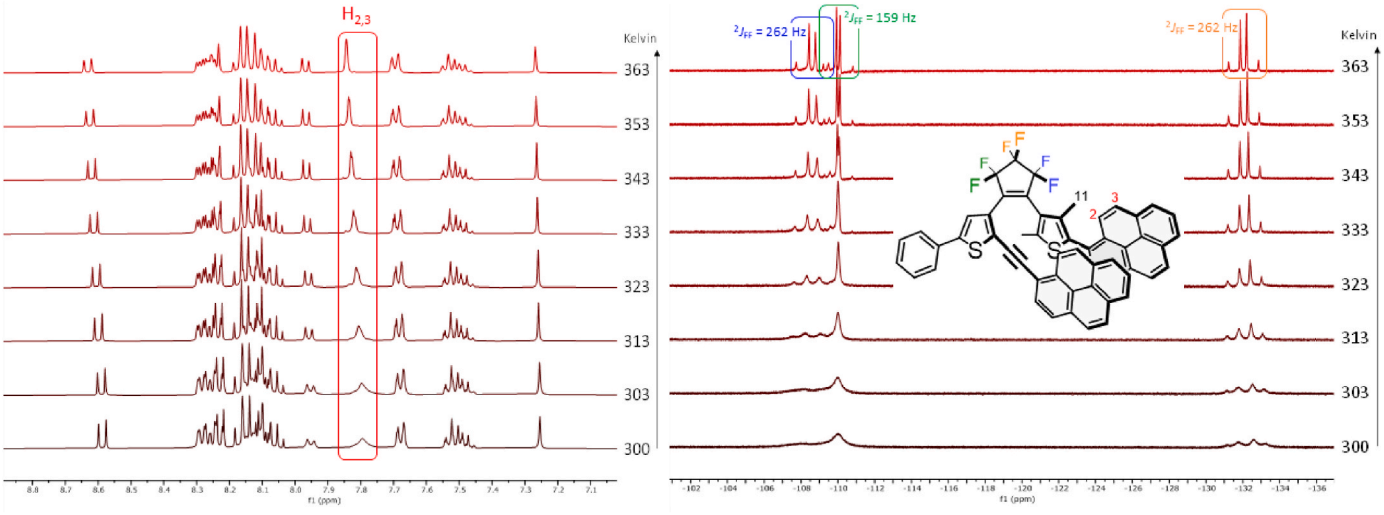

Fig. 1. *left:* Variable temperature ^{1}H NMR (500 MHz) and *right*: ^{19}F (376 MHz) spectra of **1** (TCE, from 300 to 363 K).

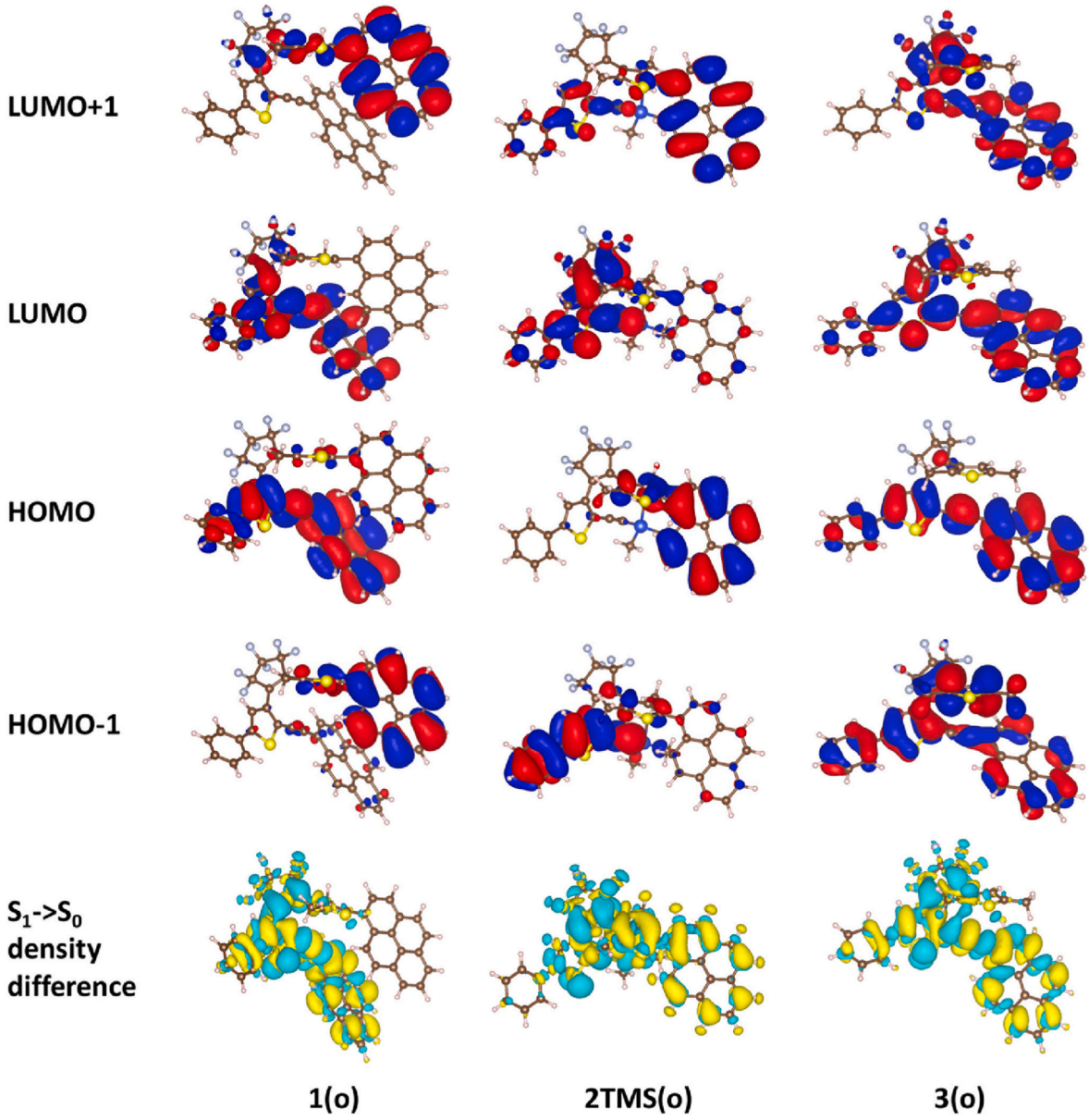

Fig. 2. Frontier molecular orbitals of the ground-state of open forms (isovalue of 0.02 au), and electronic density difference corresponding to the de-excitation (isovalue of 5.10^{-4} au).

This shift is likely attributed to an additional transition, potentially caused by supramolecular π-π interactions between pyrene units. However, the first computed excitation in **1(o)** corresponds to a π-π* transition from the HOMO to the LUMO, which is strongly delocalized along the interior DTE-acetylene-pyrene pathway, similar to that observed in **3 (o)** (see Table S2). In **2TMS(o)** the first HOMO-LUMO excitation is found to be a charge transfer transition from the pyrene to the DTE core, with a low oscillator strength due to the less efficient delocalization between those two moieties. In this system the intense absorption band recorded in the 350–375 nm range is thus attributed to the S_0- > S_2 excitation computed at 359 nm (see Table S2) and corresponding to a HOMO to LUMO+1 transition mostly involving the pyrene moiety.

Compounds **1**, **2TMS**, and **3** display a photochromic behavior upon exposure to 365 nm light in a dichloromethane solution (Fig. 3). Upon irradiation, the solutions undergo a color change to blue, for **1** and **2TMS**, or pink, for **3**, accompanied by the appearance of a distinctive broad absorption band in the visible spectrum. This band is attributed to the $S_0 \rightarrow S_1$ transition, which is centered on the closed DTE core (HOMO-LUMO computed transition, see Table S2 and Fig. S9). The anticipated $S_0 \rightarrow S_2$ transition is faintly discernible for compounds **1(c)** and **2TMS** (PSS) at around 400–430 nm but is hidden by lower-lying transitions in the case of **3**. The absorption spectrum of the isolated pure closed form **1 (c)** evidenced that upon the photocylisation reaction the lower-lying transitions of the open form, assigned to electronic delocalization along the inner thiophen-alkyne-pyrene arm, disappear with the formation of a sp^3 carbon (reactive carbon). As a consequence: i) the HOMO-1 and LUMO+1 of all three closed isomers (Fig. S9) are found to be located solely on the (acetylene-)pyrene unit and the corresponding π-π* electronic transition is found higher in energy and intense in all case, ii) several excitations are computed in between the low energy DTE centered band and this high energy pyrene-centered one, corresponding to DTE/pyrene CT excitations (Table S2 and Fig. S9). One can notice that all compounds undergo a quantitative regeneration of the initial spectra by irradiating with visible light ($\lambda = 580$ nm for **1** and **2**, $\lambda = 500$ nm for **3**), as hinted by the DTE-centered nature of the corresponding computed first excited state. Fatigability tests on compound **1** reveal a slight

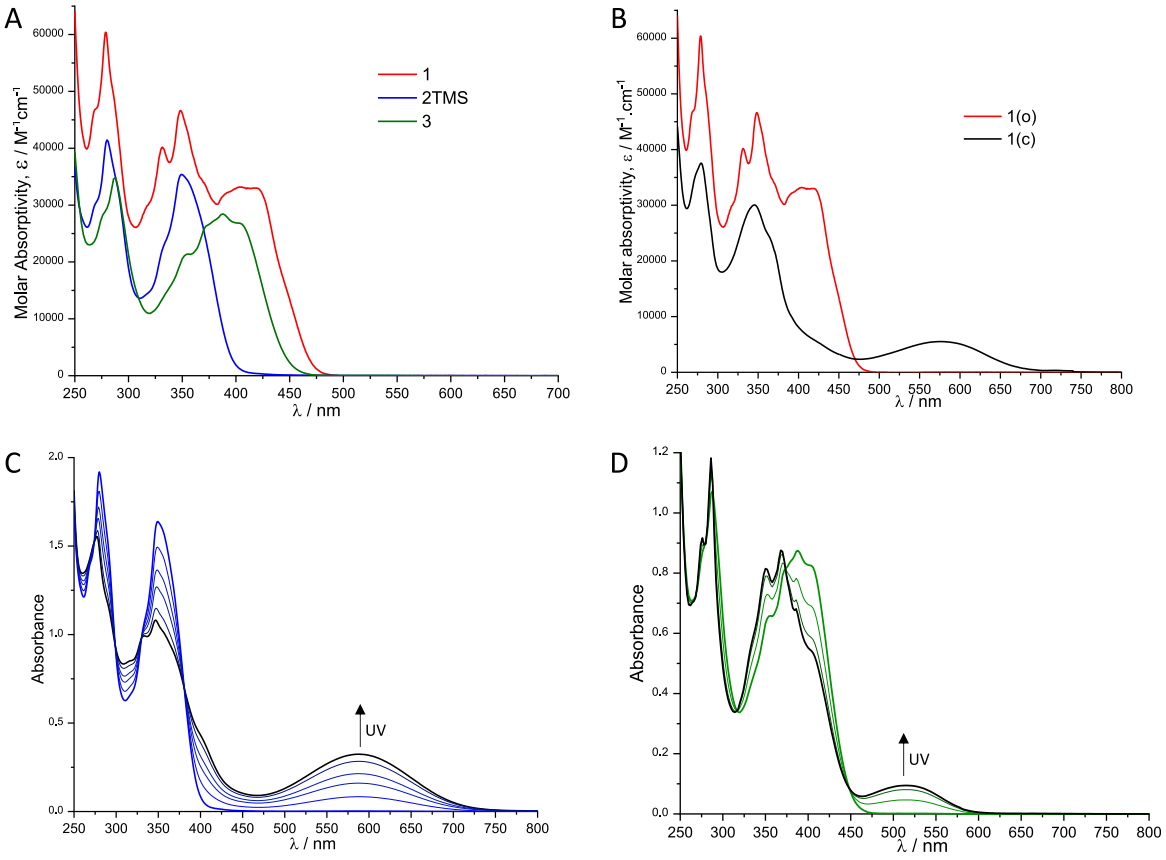

Fig. 3. Absorption spectra recorded in CH_2Cl_2 at 298 K with C ≈ 10^{-5} M of: A) **1(o)** (red line), **2TMS(o)** (blue line) and **3(o)** (green line); B) **1(o)** (red line) and isolated **1(c)** (dark line); C) and D) **2TMS** and **3** upon 365 nm light irradiation, respectively.

Table 1
Absorption and emission data for **1**, **2TMS** and **3**.

	Open form		PSS (λ_{irr} = 365 nm)		
Cpd	λ_{abs}[a] [nm] ($\varepsilon \times 10^3$ [$M^{-1}cm^{-1}$])	λ_{em}[a,b] [nm] *(PLQY [%])*	λ_{abs}[a] [nm] ($\varepsilon \times 10^3$ [$M^{-1}cm^{-1}$])	Conversion[c] [%]	$\Phi_{o\to c}$ (365 nm) $\Phi_{c\to o}$ (580 nm)
1	279 (60.3), 331 (40.2), 348 (46.6), 403 (33.2), 422 (32.8)	*515 (25)*	279 (37.3), 345 (30.0), 368sh (22.7), 426 (5.0), 577 (5.5)	35	0.012 ± 0.001 0.015 ± 0.002
2TMS	280 (41.3), 333sh (23.0), 350 (34.4)	/	276, 331, 347, 404sh, 587	65	0.047 ± 0.005 0.104 ± 0.010
3	286 (34.5), 353 (21.3), 372 (26.2), 387 (28.5), 405 (26.7)	*517 (13)*	276, 285, 350, 369, 386, 406, 516	42	0.010 ± 0.001 0.008 ± 0.001

[d] Photochromic quantum yields determined under irradiation at 365 and 580 nm (error intervals estimated from 10 % uncertainty on power and epsilon measurements).
[a] In dichloromethane solution (C ≈ 10^{-5} M) at 298 K.
[b] λ_{ex} = 365 nm.
[c] Estimated from ^{1}H NMR experiments.

decrease in reversibility over ten photochromic cycles (Fig. S12).

Photochromic conversion yields were assessed by monitoring ^{1}H NMR spectroscopic signals during light irradiation (Figs. S3–S6). The stacked ^{1}H NMR spectra of **1** exhibit that at the PSS, the signal of hydrogen H_1 in **1(c)** is distinctly visible at δ = 6.95 ppm. Additionally, the modification of the signals of the methyl groups Me_{11} (δ = 2.44 ppm) and Me_{12} (δ = 1.86 ppm) are noteworthy. Based on the relative integrations of these signals, the photocyclization reaction resulted in a 35 % conversion yield for **1**. Upon exposure to visible light at λ = 580 nm, the ^{1}H NMR spectrum of the open form **1(o)** was fully restored, indicating good reversibility and no degradation during UV light irradiation. While compound **3** exhibits a similar conversion yield (42 %), a significantly higher percentage of closed isomer is obtained for **2TMS** (65 %), reflecting the detrimental impact of the presence of the alkyne-pyrene at the inner position on the photochromic reactivity.

The ring-closure and ring-opening photokinetics were recorded under continuous irradiation at 365 nm and 575 nm, respectively (Fig. S14). The resulting time-profiles were analyzed numerically, providing the photochromic quantum yield $\Phi_{o\to c}$ and $\Phi_{c\to o}$ (Table 1). The low photocyclization quantum yields of **1**, in line with the moderate conversion yield, can be impeded to high electronic delocalization along the inner thiophene-alkyne-pyrene "arm" which introduces a strong perturbation of the expected DTE-centered LUMO (see Fig. 2), in addition to the steric hindrance resulting from the high thiophene-pyrene torsion in the lateral position. The quantum yield corresponding to the cycloreversion reaction, induced at 580 nm is in the range of the commonly observed $\Phi_{c\to o}$ for DTE derivatives. A 4-fold increase of $\Phi_{o\to c}$ is observed for **2TMS**, while DTE **3** presents similar photokinetic value as for **1**, demonstrating once again that the presence of inner alkyne-pyrene drives the photo-activity of these systems.

The emission spectra of **1** and **3** were measured under excitation at

365 nm in solutions sufficiently diluted ($<10^{-5}$ M) to exclude intermolecular excimer emission (Fig. 4 A and Fig. S13). One can notice that **2TMS** does not show significant emission, due to the substantial competition of the process with photochromism. **1** emits efficiently in the green area with an emission maximum centered around 515 nm and an absolute quantum yield of 0.25 which is 4–5 times higher than that the one reported by some of us [24] and Hashimoto et al. [18] for similar pyrene-based DAEs. The emission spectrum of compound **3** is very similar to that of compound **1**. However, it exhibits a lower photoluminescence quantum yield (PLQY) of 13 %. This reduced PLQY can reasonably be attributed to the absence of the second appended pyrene unit. In compound **1**, the presence of two pyrene units likely minimizes non-radiative deactivation pathways through rotational constraint and energy stabilization. Interestingly, based on the similar emission features observed between compounds **1** and **3**, it can be concluded that an excimer state is not likely to be present in compound **1**. Instead, the thienyl-acetylene-pyrene fragment in both compounds is more likely responsible for the observed luminescence. Functionalization of the pyrene at the 1-position provides intense electronic delocalization throughout the entire internal arm, thereby establishing a pathway for radiative deactivation. **1(o)** and **3(o)** possess very similar computed emission energy (see Table S2), in agreement with the recorded spectra, with an intense de-excitation from the lowest excited state delocalized on the DTE arm and the acetylene-pyrene unit (see Fig. 2 for a representation of the S_1- > S_0 de-excitation as an electronic density difference). In parallel, the non-emissive character of **2TMS(o)** and the preponderance of the ring closure form the first excited state can thus also be linked to the charge transfer (DTE to pyrene) nature of the lowest computed electronic transition, with a near-zero oscillator strength (see Fig. 2 and Table S2), impeding the radiative de-excitation.

As expected, the emission intensity of **1** decreases upon continuous irradiation at 365 nm, due to the concomitant photocyclization process (Fig. 4 B). A weak structured emission band from 375 to 450 nm emerges, with a vibrational spacing of 1283 cm^{-1} (of the $S_1 \rightarrow S_0$ transition), typical of the monomeric emission of pyrene. This higher-energy emission is reasonably attributed to the small amount of the parallel conformer in the solution. The impact of the photo-switching process on the emission is also observed for **3**. For both systems **1** and **3**, the decrease in emission intensity upon the photocyclization reaction is attributed to changes in electronic factors centered on the internal arm. Specifically, the cyclization reaction generates hybridized sp^3 carbons that, in the case of the alkyne-substituted pyrene arm, disrupt electronic delocalization.

Two-photon excitation (TPE) measurements of compounds **1** and **3** were conducted to investigate the potential for non-destructive readout applications (Fig. 4C, S15 and S18-19). The nonlinear process of two-photon absorption can selectively produce luminescence without triggering photochromism [24]. The TPE emission was recorded under 730 nm light excitation with an incident power of 90 mW, over a 5-s acquisition period. In Fig. 4C, **1** shows a broad TPE emission, with identical shape and λ_{max} as one-photon emission (515 nm). Such emission remained stable throughout the 20 min measurement duration, without evidence of the formation of the closed isomer, thus demonstrating the selective radiative deactivation pathway upon nonlinear excitation.

For both compounds **1** and **3**, the two-photon absorption (TPA) cross-sections are relatively low, ranging from $\sigma 2 = 50$–60 GM at 700–730 nm (Figs. S18 and S19). This is typical for mono-functionalized pyrene

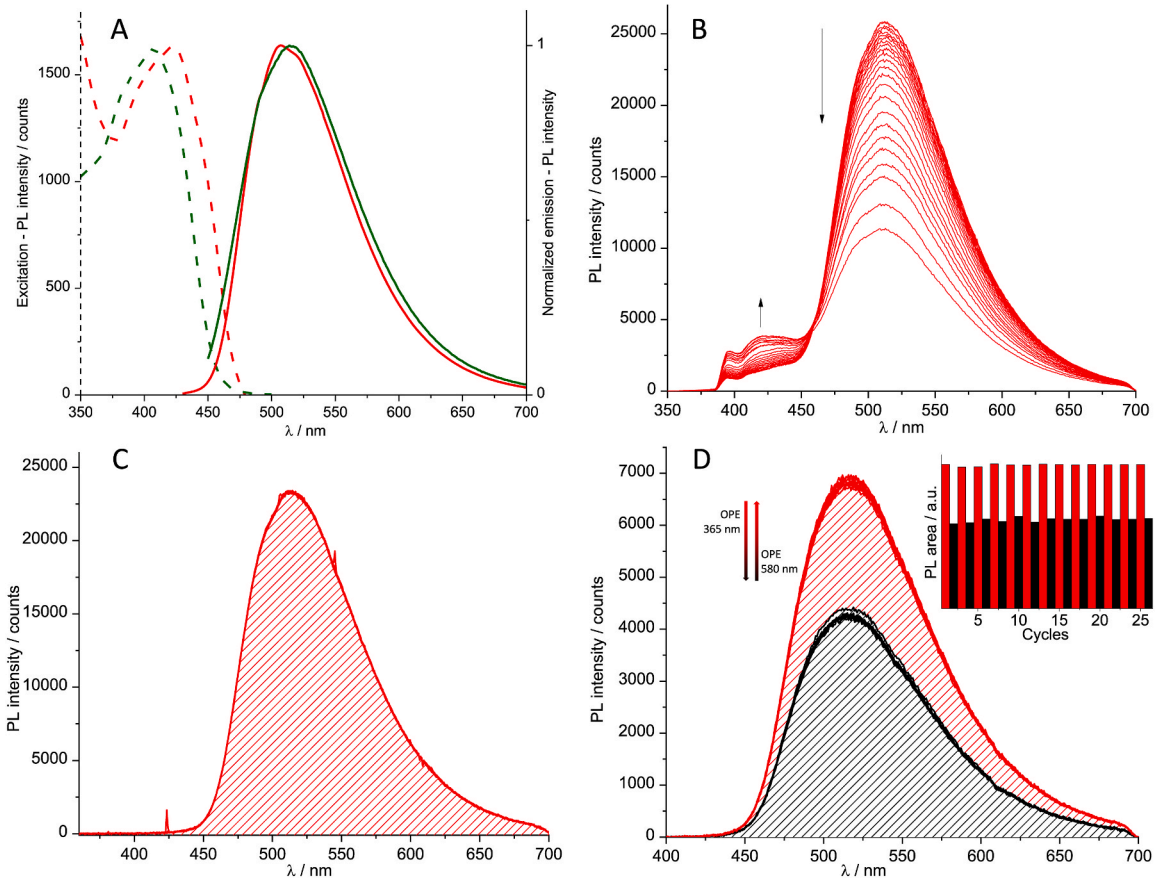

Fig. 4. A) Emission (solid line) and excitation (dashed line) spectra of **1(o)** (red line) and **3(o)** (green line). Evolution of the emission of **1(o)** upon: B) continuous one photon excitation at 365 nm and C) two-photon excitation at 730 nm. D) Cyclic of one- and two-photon excitations, with alternation of 365 nm and 580 nm for triggering the photochromic reaction in one-photon excitation.

motifs [40,41]. However, these low cross-sections do not pose a challenge for this study, as the focus is on the potential modulation of the TPA signal with high contrast, rather than on achieving high absolute TPA values.

As expected, orthogonal OPE excitation at 365 nm on the same solution triggered the photocyclization reaction. The TPE signal recorded in the solution at the PSS was found to be diminished by a factor of 1.6 (Fig. 4D). Orthogonal white light irradiation fully recovered the initial open form, restoring the initial TPE signal intensity of the open isomer. Perfect fatigue resistance was observed over 25 cycles, with a stable "on"/"off" TPE contrast of 46 % (Fig. 4D, inset). One can notice that no evidence of a TPE-activated cycloreversion reaction was observed during 730 nm excitation of the solution at the PSS.

Compound **3(o)** exhibits TPE emission at a similar energy level to that of **1(o)**, with slight changes in the emission shape (Fig. S15), consequently to the similarities of their electronic structure and OPE emission. Interestingly, **3(o)** undergoes a photocyclization reaction under TPE excitation (Fig. S16). At high excitation power, the photocyclization process induces a deviation from the quadratic response (Fig. S18). This behavior highlights the beneficial effect of the second pyrene in compound **1**, which facilitates the radiative deactivation pathway prior to the photocyclization reaction. Similar to **1(o)**, the photoisomerization reaction of **3(o)** upon OPE (365 nm) to the PSS state led to a decrease in the TPE signal. The "on"/"off" TPE contrast of **3** drops to 17 % compared to **1(o)** (Fig. S17), demonstrating the beneficial effect of the two pyrene units on the combined OPE/TPE photophysical processes.

4. Conclusion

We report herein an effective photo-switchable all-optical non-destructive molecular system. This system features an innovative design in which two pyrenes are asymmetrically attached to a dithienylethene core, extensively characterized using NMR spectroscopy. The two-photon excitation (TPE) output signal is photo-modulated with a contrast of 46 % and exhibits excellent fatigability when exposed to one-photon excitation (OPE) light at either 365 nm or 580 nm. Theoretical studies indicate that the internal functionalization of pyrene is responsible for the observed photoactivity in these systems through the extended π-conjugated pathway brought by an excellent electronic communication with the DTE arm, while the external pyrene is constrained in a twisted orientation and is more isolated electronically. However, these constraints in the structure, where intramolecular interactions between the pyrene moieties reduce degrees of freedom and limit non-radiative deactivation pathways, ultimately results in the superior photophysical properties observed for **1**.

CRediT authorship contribution statement

Marie Barale: Investigation, Formal analysis, Conceptualization. **Iulia Turcas:** Investigation. **Violette Gousseau:** Investigation. **Muriel Escadeillas:** Investigation. **Elsa Caytan:** Writing – original draft, Investigation, Formal analysis, Data curation. **Gregory Taupier:** Investigation. **Yann Molard:** Writing – original draft, Investigation, Data curation. **Arnaud Fihey:** Writing – review & editing, Writing – original draft, Validation, Supervision, Project administration, Methodology, Investigation, Funding acquisition, Formal analysis, Data curation, Conceptualization. **Julien Boixel:** Writing – review & editing, Writing – original draft, Visualization, Validation, Supervision, Project administration, Methodology, Investigation, Funding acquisition, Formal analysis, Data curation, Conceptualization.

Declaration of competing interest

The authors declare that they have no known competing financial interests or personal relationships that could have appeared to influence the work reported in this paper.

Data availability

Data will be made available on request.

Acknowledgements

This work was supported by financial supports from the CNRS and the University of Rennes. The authors are grateful to the EUR LUMOMAT project and the Investments for the Future program ANR-18-EURE-0012. Part of this work has been performed using the PRISM core facility (Biogenouest, Univ Rennes, Univ Angers, INRAE, CNRS, FRANCE). Dr. Marie Dallon is acknowledged for X-ray diffraction studies. The authors are grateful to the analytical center CRMPO for the elemental and HRMS analyses.

Appendix A. Supplementary data

Supplementary data to this article can be found online at https://doi.org/10.1016/j.dyepig.2024.112473.

References

[1] Carling C-J, Boyer J-C, Branda NR. Multimodal fluorescence modulation using molecular photoswitches and upconverting nanoparticles. Org Biomol Chem 2012; 10:6159–68. https://doi.org/10.1039/C2OB25368B.
[2] Fukaminato T, Doi T, Tamaoki N, Okuno K, Ishibashi Y, Miyasaka H, et al. Single-molecule fluorescence photoswitching of a Diarylethene−Perylenebisimide dyad: non-destructive fluorescence readout. J Am Chem Soc 2011;133:4984–90. https://doi.org/10.1021/ja110686t.
[3] Irie M, Fukaminato T, Sasaki T, Tamai N, Kawai T. A digital fluorescent molecular photoswitch. Nature 2002;420:759–60. https://doi.org/10.1038/420759a.
[4] Leydecker T, Herder M, Pavlica E, Bratina G, Hecht S, Orgiu E, et al. Flexible non-volatile optical memory thin-film transistor device with over 256 distinct levels based on an organic bicomponent blend. Nat Nanotechnol 2016;11:769–75. https://doi.org/10.1038/nnano.2016.87.
[5] Naren G, Larsson W, Benitez-Martin C, Li S, Pérez-Inestrosa E, Albinsson B, et al. Rapid amplitude-modulation of a diarylethene photoswitch: en route to contrast-enhanced fluorescence imaging. Chem Sci 2021;12:7073–8. https://doi.org/10.1039/D1SC01071A.
[6] Tsivgoulis GM, Lehn J-M. Multiplexing optical systems: multicolor-bifluorescent-biredox photochromic mixtures. Adv Mater 1997;9:627–30. https://doi.org/10.1002/adma.19970090806.
[7] Zhong W, Shang L. Photoswitching the fluorescence of nanoparticles for advanced optical applications. Chem Sci 2024;15:6218–28. https://doi.org/10.1039/D4SC00114A.
[8] Li Z, Zeng X, Gao C, Song J, He F, He T, et al. Photoswitchable diarylethenes: from molecular structures to biological applications. Coord Chem Rev 2023;497: 215451. https://doi.org/10.1016/j.ccr.2023.215451.
[9] Irie M, Fukaminato T, Matsuda K, Kobatake S. Photochromism of diarylethene molecules and crystals: memories, switches, and actuators. Chem Rev 2014;114: 12174–277. https://doi.org/10.1021/cr500249p.
[10] Zhang Z, Zhang J, Wu B, Li X, Chen Y, Huang J, et al. Diarylethenes with a narrow singlet–triplet energy gap sensitizer: a simple strategy for efficient visible-light photochromism. Adv Opt Mater 2018;6:1700847. https://doi.org/10.1002/adom.201700847.
[11] Harvey EC, Feringa BL, Vos JG, Browne WR, Pryce MT. Transition metal functionalized photo- and redox-switchable diarylethene based molecular switches. Coord Chem Rev 2015;282–283:77–86. https://doi.org/10.1016/j.ccr.2014.06.008.
[12] Norsten TB, Peters A, McDonald R, Wang M, Branda NR. Reversible [7]-Thiahelicene formation using a 1,2-dithienylcyclopentene photochrome. J Am Chem Soc 2001;123:7447–8. https://doi.org/10.1021/ja015988r.
[13] Liddell PA, Kodis G, Moore AL, Moore TA, Gust D. Photonic switching of photoinduced electron transfer in a Dithienylethene−Porphyrin−Fullerene triad molecule. J Am Chem Soc 2002;124:7668–9. https://doi.org/10.1021/ja026327c.
[14] Ikariko I, Kim S, Hiroyasu Y, Higashiguchi K, Matsuda K, Hirose T, et al. All-visible (>500 nm)-Light-Induced diarylethene photochromism based on multiplicity conversion via intramolecular energy transfer. J Phys Chem Lett 2022;13:7429–36. https://doi.org/10.1021/acs.jpclett.2c01903.
[15] Bag SK, Pal A, Jana S, Thakur A. Recent advances on diarylethene-based photoswitching materials: applications in bioimaging, controlled singlet oxygen generation for photodynamic therapy and catalysis. Chem Asian J 2024: e202400238. https://doi.org/10.1002/asia.202400238. n/a.
[16] Wu Y, Zhu Y, Yao C, Zhan J, Wu P, Han Z, et al. Recent advances in small-molecule fluorescent photoswitches with photochromism in diverse states. J Mater Chem C 2023;11:15393–411. https://doi.org/10.1039/D3TC02383D.

[17] Zhang J, Tian H. The endeavor of diarylethenes: new structures, high performance, and bright future. Adv Opt Mater 2018;6:1701278. https://doi.org/10.1002/adom.201701278.
[18] Hashimoto Y, Nakashima T, Shimizu D, Kawai T. Photoswitching of an intramolecular chiral stack in a helical tetrathiazole. Chem Commun 2016;52:5171–4. https://doi.org/10.1039/C6CC01277A.
[19] Baggi N, Garoni E, Colombo A, Dragonetti C, Righetto S, Roberto D, et al. Design of cyclometallated 5-π-delocalized donor-1,3-di(2-pyridyl)benzene platinum(II) complexes with second-order nonlinear optical properties. Polyhedron 2018;140:74–7. https://doi.org/10.1016/j.poly.2017.11.051.
[20] Roberts MN, Nagle JK, Finden JG, Branda NR, Wolf MO. Linker-dependent metal-sensitized photoswitching of dithienylethenes. Inorg Chem 2009;48:19–21. https://doi.org/10.1021/ic801619v.
[21] Zhao H, Garoni E, Roisnel T, Colombo A, Dragonetti C, Marinotto D, et al. Photochromic DTE-substituted-1,3-di(2-pyridyl)benzene platinum(II) complexes: photomodulation of luminescence and second-order nonlinear optical properties. Inorg Chem 2018;57:7051–63. https://doi.org/10.1021/acs.inorgchem.8b00733.
[22] Browne WR, Feringa BL. Making molecular machines work. Nat Nanotechnol 2006;1:25–35. https://doi.org/10.1038/nnano.2006.45.
[23] The Fundamentals of Making Mechanical Bonds. The nature of the mechanical bond. John Wiley & Sons, Ltd; 2016. p. 55–268. https://doi.org/10.1002/9781119044123.ch2.
[24] Barale M, Escadeillas M, Taupier G, Molard Y, Orione C, Caytan E, et al. Nondestructive all-optical readout through photoswitching of intramolecular excimer emission. J Phys Chem Lett 2022;13:10936–42. https://doi.org/10.1021/acs.jpclett.2c02960.
[25] Mori K, Ishibashi Y, Matsuda H, Ito S, Nagasawa Y, Nakagawa H, et al. One-color reversible control of photochromic reactions in a diarylethene derivative: three-photon cyclization and two-photon cycloreversion by a near-infrared femtosecond laser pulse at 1.28 μm. J Am Chem Soc 2011;133:2621–5. https://doi.org/10.1021/ja108992t.
[26] Arai Y, Ito S, Fujita H, Yoneda Y, Kaji T, Takei S, et al. One-colour control of activation, excitation and deactivation of a fluorescent diarylethene derivative in super-resolution microscopy. Chem Commun 2017;53:4066–9. https://doi.org/10.1039/C6CC10073B.
[27] Sotome H, Nagasaka T, Une K, Okui C, Ishibashi Y, Kamada K, et al. Efficient cycloreversion reaction of a diarylethene derivative in higher excited states attained by off-resonant simultaneous two-photon absorption. J Phys Chem Lett 2017;8:3272–6. https://doi.org/10.1021/acs.jpclett.7b01388.
[28] Kashihara R, Morimoto M, Ito S, Miyasaka H, Irie M. Fluorescence photoswitching of a diarylethene by irradiation with single-wavelength visible light. J Am Chem Soc 2017;139:16498–501. https://doi.org/10.1021/jacs.7b10697.
[29] Sotome H, Nagasaka T, Konishi T, Kamada K, Morimoto M, Irie M, et al. Near-infrared two-photon absorption and excited state dynamics of a fluorescent diarylethene derivative. Photochem Photobiol Sci 2024;23:1041–50. https://doi.org/10.1007/s43630-024-00573-y.
[30] Kobayashi Y, Mutoh K, Abe J. Stepwise two-photon absorption processes utilizing photochromic reactions. J Photochem Photobiol C Photochem Rev 2018;34:2–28. https://doi.org/10.1016/j.jphotochemrev.2017.12.006.
[31] Burns KH, Quincy TJ, Elles CG. Excited-state resonance Raman spectroscopy probes the sequential two-photon excitation mechanism of a photochromic molecular switch. J Chem Phys 2022;157:234302. https://doi.org/10.1063/5.0126974.
[32] Nagasaka T, Kunishi T, Sotome H, Koga M, Morimoto M, Irie M, et al. Multiphoton-gated cycloreversion reaction of a fluorescent diarylethene derivative as revealed by transient absorption spectroscopy. Phys Chem Chem Phys 2018;20:19776–83. https://doi.org/10.1039/C8CP01467A.
[33] de Reguardati S, Pahapill J, Mikhailov A, Stepanenko Y, Rebane A. High-accuracy reference standards for two-photon absorption in the 680–1050 nm wavelength range. Opt Express 2016;24. https://doi.org/10.1364/OE.24.009053. 9053–66.
[34] Frisch MJ, Trucks GW, Schlegel HB, Scuseria GE, Robb MA, Cheeseman JR, Scalmani G, Barone V, Petersson GA, Nakatsuji H, Li X, Caricato M, Marenich AV, Bloino J, Janesko BG, Gomperts R, Mennucci B, Hratchian HP, Ortiz JV, Izmaylov AF, Sonnenberg JL, Williams, Ding F, Lipparini F, Egidi F, Goings J, Peng B, Petrone A, Henderson T, Ranasinghe D, Zakrzewski VG, Gao J, Rega N, Zheng G, Liang W, Hada M, Ehara M, Toyota K, Fukuda R, Hasegawa J, Ishida M, Nakajima T, Honda Y, Kitao O, Nakai H, Vreven T, Throssell K, Montgomery Jr JA, Peralta JE, Ogliaro F, Bearpark MJ, Heyd JJ, Brothers EN, Kudin KN, Staroverov VN, Keith TA, Kobayashi R, Normand J, Raghavachari K, Rendell AP, Burant JC, Iyengar SS, Tomasi J, Cossi M, Millam JM, Klene M, Adamo C, Cammi R, Ochterski JW, Martin RL, Morokuma K, Farkas O, Foresman JB, Fox DJ. Gaussian 16 rev. A.03. 2016. n.d.
[35] Adamo C, Barone V. Toward reliable density functional methods without adjustable parameters: the PBE0 model. J Chem Phys 1999;110:6158–70. https://doi.org/10.1063/1.478522.
[36] Scalmani G, Frisch MJ. Continuous surface charge polarizable continuum models of solvation. I. General formalism. J Chem Phys 2010;132:114110. https://doi.org/10.1063/1.3359469.
[37] Crawford AG, Dwyer AD, Liu Z, Steffen A, Beeby A, Pålsson L-O, et al. Experimental and theoretical studies of the photophysical properties of 2- and 2,7-functionalized pyrene derivatives. J Am Chem Soc 2011;133:13349–62. https://doi.org/10.1021/ja2006862.
[38] Yang S-W, Elangovan A, Hwang K-C, Ho T-I. Electronic polarization reversal and excited state intramolecular charge transfer in donor/acceptor ethynylpyrenes. J Phys Chem B 2005;109:16628–35. https://doi.org/10.1021/jp052086u.
[39] Coleman A, Pryce MT. Synthesis, electrochemistry, and photophysical properties of a series of luminescent pyrene-thiophene dyads and the corresponding Co2(CO)6 complexes. Inorg Chem 2008;47:10980–90. https://doi.org/10.1021/ic801226p.
[40] Kim HM, Lee YO, Lim CS, Kim JS, Cho BR. Two-photon absorption properties of alkynyl-conjugated pyrene derivatives. J Org Chem 2008;73:5127–30. https://doi.org/10.1021/jo800363v.
[41] Abeywickrama CS, Wijesinghe KJ, Plescia CB, Fisher LS, Goodson Iii T, Stahelin RV, et al. A pyrene-based two-photon excitable fluorescent probe to visualize nuclei in live cells. Photochem Photobiol Sci 2020;19:1152–9. https://doi.org/10.1039/D0PP00107D.